ACS APPLIED BIO MATERIALS Cite This: ACS Appl. Bio Mater. XXXX, XXX, XXX−XXX

Article

www.acsabm.org

Influence of Transition Metal Dichalcogenide Surfaces on Cellular Morphology and Adhesion

Anthony Palumbo,[†] Filippos Tourlomousis,[†,‡] Robert C. Chang,[†] and Eui-Hyeok Yang*[,†]

[†]Department of Mechanical Engineering, Stevens Institute of Technology, Hoboken, New Jersey 07030, United States

[‡]The Center for Bits and Atoms, Massachusetts Institute of Technology, Cambridge, Massachusetts 02138, United States

Supporting Information

ABSTRACT: This article presents the effect of transition metal dichalcogenide (TMD) surfaces and their geometric arrangements on resulting cellular morphology and adhesion. WS_2 and MoS_2 on SiO_2 and polydimethylsiloxane (PDMS) substrates were utilized as cell culture platforms, and cell−substrate interactions were probed via analysis of cellular morphometric features (i.e., cell area and circularity) of neonatal human dermal fibroblasts (NHDFs) and metrology of TMD surfaces. It was quantitatively confirmed that the presence of TMDs on substrates resulted in an overall enhanced cellular morphology, even on SiO_2 substrates adverse to cellular adhesion. On a localized scale, distinct TMD geometric features at sites of adhesion were measured and correlated with the observed cell morphology. Geometric parameters of TMDs, including TMD island count and total TMD area, exhibited positive correlations with the resulting morphology of cells by enhancing cellular areas and elongations. Further, geometric properties were compared to cell area per TMD island, and positive correlations were observed with TMD island size parameters. Cells adhered at heterogeneous locations with combinations of exposed TMD and SiO_2, demonstrating an enhanced morphology in relation to the number of TMD islands in a cell's local area and the geometric size parameters of TMD islands within the cell's operating length scale. The proposed mechanisms of cellular adhesion on TMD-modified surfaces are attributed to the role of surface properties (e.g., stiffness, friction, and hydrophobicity) of TMD and underlying SiO_2 and their combined effects during progressive stages of cellular adhesion. These findings provide insight toward possibilities of tailoring adhesion of cells guided by geometric parameters of TMDs.

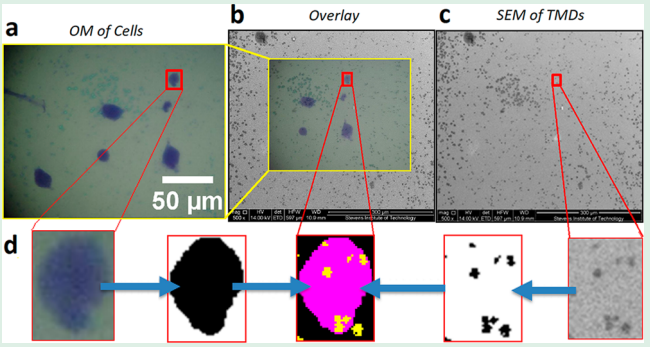

KEYWORDS: *transition metal dichalcogenides, fibroblast cells, biotic/abiotic interfaces, cell adhesion, 2D cell culture*

INTRODUCTION

Two-dimensional (2D) materials have been widely explored for their unique electronic, mechanical, and catalytic properties.[1−7] Owing to the high surface-to-volume ratio and structural rigidity, 2D materials allow maximal interaction between their surfaces and environment within small sample volumes for rapid performance and high sensitivity.[8,9] Transition metal dichalcogenides (TMDs) such as molybdenum disulfide (MoS_2) and tungsten disulfide (WS_2) are unique as semiconducting analogues to graphene, which undergo an indirect to direct band gap transition when thinned down to a monolayer,[10] enabling a high electronic sensitivity and photoluminescence capability toward biosensing and bioimaging applications,[11] highly sensitive DNA sequencing,[12,13] and photothermal therapy (PTT).[14,15] Significant work has been pursued to integrate some of these unique properties of TMDs for biomedical fields, including drug delivery, therapeutics, biosensors, and bioimaging.[16−19] Coinciding with developments of TMD synthesis, many of these studies involve TMDs suspended in solutions.[18−20] On the other hand, ongoing efforts in TMD synthesis have enabled greater capabilities in utilizing TMD surfaces,[19−21] and consequently, emerging cell-based device platforms are governed by cell adhesion on TMD-modified surfaces, including MoS_2 nanosheets assembled in thin films and scaffolds used to: induce neural stem cell differentiation at a high efficiency,[22] improve mechanical reinforcement,[23] reinforce bioceramic scaffolds,[24] and treat malignant bone tumors.[25] Monolayer TMDs, such as MoS_2 and WS_2, are unique semiconducting two-dimensional crystals with superior material properties and demonstrable biocompability, owing to their emergence as a promising class of biomaterials to achieve new capabilities and improve strategies and performance indicators of existing technologies and devices. Despite progress, studies characterizing the influences of TMD surfaces in applications involving cellular growth are not well reported.

One of the issues concerning adaptation of biological cells to their environment involves their adhesive interaction with their respective substrate. The incorporation of TMDs with biological

Received: August 7, 2018
Accepted: October 17, 2018
Published: October 17, 2018

DOI: 10.1021/acsabm.8b00405
ACS Appl. Bio Mater. XXXX, XXX, XXX−XXX

systems needs an understanding of the role of TMDs on cell adhesion. Cellular adhesion to cell substrates precedes and influences subsequent aspects of cellular physiology, including survival, proliferation, migration, and differentiation.[26] Thus, understanding of the influence of TMDs on biological cell adhesion is important in facilitating the control and manipulation of desirable cellular responses involving 2D cell culture platforms,[16−18,20,27] as has been demonstrated with the enhancement of cell differentiation with patterning graphene.[28]

To date, various attempts have been pursued to assess cell viability with TMDs, particularly relating to the material's potential cytotoxicity. Preliminary in vivo toxicology tests on mammals demonstrated the potential of employing TMDs within living subjects.[29] The biocompatibility of TMDs suspended in solutions has been probed in its multiple forms, including TMD nanoparticles,[30] TMD nanotubes,[31] and chemically exfoliated few layered TMD nanosheets,[32,33] all of which indicated cytocompatibility of TMDs dispersed in solutions. Though most of cytotoxicity studies have focused on TMDs in dispersions, emerging cell-based device platforms are governed by cell adhesion on the TMD-modified surface. Recently, cells were cultured on TMD surfaces, including 2+ layered nanosheets of mechanically exfoliated and chemical vapor deposition (CVD)-grown TMDs, and cell viability was evaluated by live−dead fluorescence labeling to detect acute toxicity and reactive oxygen species to monitor for apoptosis.[34] Further, MoS_2 and WS_2 have been coated on cell culture substrates by the drop-casting method, demonstrating a low cytotoxicity and enhanced morphology.[35] While these studies show a promising cytocompatibility of TMDs, probing cytocompatibility without considerations of size and spatial arrangements of TMD-modified surfaces does not account for the parametric influences of TMDs on cellular adhesion. Here we present the first report addressing spatial considerations of 2D TMD surfaces and their influence on resulting cellular morphology and adhesion. We show the influence of TMDs on the adhesive behavior of mammalian cells by quantitatively analyzing the morphometric features (i.e., circularity and cell area) of the adhered cells. We grow predominantly monolayer WS_2 and MoS_2 via CVD on SiO_2 substrates and transfer them onto PDMS substrates. We then seed these substrates with neonatal human dermal fibroblasts (NHDFs) for quantitative analysis of the resulting cellular morphometric features and compare the effects of TMD presence on the adherence of fibroblast cells. Finally, we correlate the geometric properties of TMD to the morphometric features of adhered cells and corroborate that the presence of TMDs and their geometric arrangements significantly improve the cellular adhesion.

EXPERIMENTAL SECTION

TMD Synthesis and Characterization. A clean 4 in. Si wafer with 90 nm thick SiO_2 was deposited with a 5 nm thick MoO_3 or WO_3 film from pellets (Sigma-Aldrich) via an electron beam evaporator (Denton Explorer) and cut into 1 cm × 1 cm areas, designating the transition metal source chips; separately, another clean 4 in. Si wafer with 90 nm thick SiO_2 was cut into 1 cm × 1 cm areas, designating the growth chips as the substrate upon which TMD monolayers are deposited. A transition metal source chip was placed face-to-face atop of a growth chip and loaded together into the center of a 3 in. diameter quartz tube within an MTI 1200X 1-zone furnace. An aluminum crucible containing 0.9 g of powdered sulfur (chalcogen source) was placed upstream for sublimation into gaseous sulfur, and a mass flow controller (Aalborg) delivered Ar at 30 sccm as an inert gas carrier from 300 °C, with a base pressure of 200 mTorr. Using the temperature controller, the TMD growth program was set up according to the following sequence: (1) maintain room temperature for 5 min to get a high vacuum degree via pumping, (2) ramp at 18 °C/min to 550 °C, (3) ramp at 6.0 °C/min to 750 °C, (4) maintain 750 °C for 25 min, and (5) cool down via natural heat dissipation to 450 °C, at which point the Ar gas was turned off and furnace opened for rapid cooling.

As shown in Figure S1a,b, Raman and photoluminescence (PL) measurements were performed using a Horiba Xplora system with an Andor iDus 420 detector with a 532 nm laser at room temperature. The spot size of the laser was approximately 1 um^2. Optical images were taken with an Olympus BX41 microscope, and SEM imaging was performed with Quanta FEG 450, FEI. Raman and PL spectra were also taken after transfer of TMD to PDMS as shown in Figure S1b,c, demonstrating quenching of PL and shifting of Raman and PL peaks. The observable peak shifts of Raman and PL are attributed to strain relaxation after transfer.[36−38] The reduction of PL intensity may be attributed to the adsorption of O_2, H_2O, or acetone/IPA molecules encountered during the transfer process.[39,40] These shifts help reveal the extent of defect introduction in the material following transfer, which can ultimately affect the surface and mechanical properties.[41]

TMD Transfer onto PDMS. After growth of TMD (i.e., MoS_2 or WS_2) on SiO_2, a wet transfer method was utilized to transfer TMD onto PDMS substrates. The samples were thoroughly cleaned via solvent cleaning to remove any residues from SiO_2 onto the PDMS substrate. The PDMS (Dow Corning, Sylgard-184) was fabricated with a ratio of 10:1 of silicone elastomer base and curing agent. First, TMD monolayers grown on SiO_2 were coated with a thin layer of poly(methyl methacrylate) (PMMA) (950 A4) via dropper and left in ambient conditions for 60 min. Upon drying, the samples were placed face-up to float in a 30% KOH aqueous solution for 15 min, allowing the oxide layer of the SiO_2 to etch away and release the underlying substrate from the PMMA/TMD. The PMMA/TMD was transferred to DI water and placed on the PDMS substrate, followed by drying in ambient conditions for 1 h and baked at 90 °C for 1 min. The PMMA was removed by 30 min exposure of acetone and then rinsed with IPA. A flowchart pertaining to the preparation of TMD samples can be viewed in Figure S2.

Cell Culture. As-grown TMDs (i.e., MoS_2 or WS_2) on SiO_2 substrates were cultured with neonatal human dermal fibroblasts (NHDFs) in high-glucose Dulbecco's modified Eagle's medium (DMEM), containing 1% penicillin/streptomycin and 10% fetal bovine serum in basal media. SiO_2 substrates without TMDs were assigned as control samples, and all samples were seeded with NHDFs at the P7 generation. NHDFs were cultured on each sample surface for 24 h at standard incubating conditions (37 °C, 5% CO_2). Cell seeding densities were optimized at 15 000 cells/cm^2 to achieve sufficient sample sizes and intercellular spacing for single cell analyses.

Cell Stain. Immediately following the 24 h culturing, fibroblast cell morphology was observed via optical microscopy (Horiba Xplora), utilizing methyl violet (Sigma-Aldrich) as a cell stain, with a representative optical image shown in Figure S3a,b. As shown in Figure S4, concentrations of methyl violet in DI water (i.e., 0.04, 0.1, 0.2, and 0.4 mg/mL) were first tested on SiO_2 control substrates (without cells). Higher concentrations resulted in supersaturation of methyl violet overtime due to solvent evaporation, as observed by the violet conglomerate formations at higher concentrations overtime. Therefore, a cell staining concentration of 0.1 mg/mL was determined based on the absence of methyl violet conglomerate formation observed after 90 min. Furthermore, the time of exposure of cells to cell stain was tested as shown in Figure S5a−d. SiO_2 control substrates were cultured as described above and exposed to the methyl violet cell stain of 0.1 mg/mL for varying durations (i.e., 30 s, 60 s, 90 s, 120 s). We determined that 120 s of exposure to the cell stain was sufficient for observing cell morphology of the adhered fibroblast cells via optical microscope.

Quantification of TMD Geometric Features and Cellular Morphometric Features. Thresholding and noise filtering algorithms were applied to the obtained optical images for segmentation of individual stained fibroblast cells using Fiji software.[42] Cellular morphometric features including total cell area and circularity were calculated and defined within Fiji. Circularity was calculated as

DOI: 10.1021/acsabm.8b00405
ACS Appl. Bio Mater. XXXX, XXX, XXX−XXX

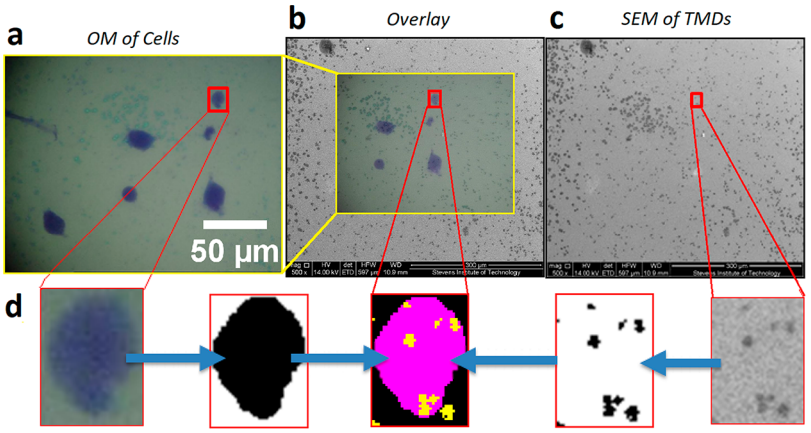

Figure 1. Representative image segmentation of fibroblast cell morphology and WS_2 on SiO_2 substrate. (a) Optical microscope image of a sample of WS_2 on SiO_2 with adherent cells stained with methyl violet. (b) Overlay image of an optical microscope image (65% transparency) and SEM image of underlying WS_2/SiO_2 for determination of the cell footprint location. (c) SEM image of underlying WS_2/SiO_2 sample location corresponding to site of cell adhesion (i.e., cell footprint). (d) Perimeter boxes drawn around the adherent fibroblast cell outline and the corresponding location on the sample, followed by segmented images and a combined colored overlay image at center, representing the following: cell morphology (purple), WS_2 (yellow), areas of overlap between WS_2 and the cell (white), and SiO_2 absent of WS_2 or cell (black).

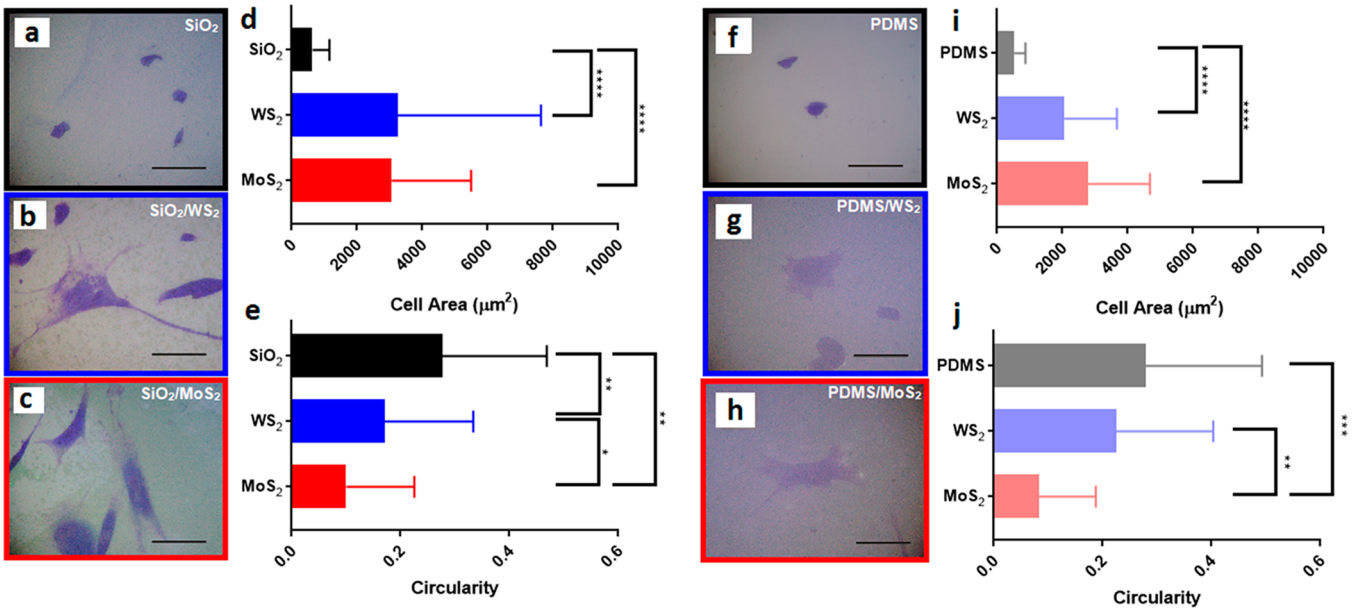

Figure 2. Cell morphology on differing TMD/substrate combinations. Representative optical microscope images of individual fibroblast cells cultured on (a) SiO_2, (b) WS_2 on SiO_2, (c) MoS_2 on SiO_2, (f) PDMS, (g) WS_2 on PDMS, and (h) MoS_2 on PDMS. Scale bar = 100 um; cells overlapping neighboring cells or spanning beyond the field of view were discarded from the analysis. Graph of morphometric features of fibroblast cells adhered on (d, e) SiO_2 substrates and (i, j) PDMS substrates with and without TMDs, including (d, i) cell area and (e, j) circularity, with statistical significances shown; mean ± SD, n = 50−60 cells (per sample), $^*P \leq 0.05$; $^{**}P \leq 0.01$, $^{***}P \leq 0.001$, $^{****}P \leq 0.0001$.

circularity = 4π(area/perimeter^2); a circularity value of 1.0 indicates a perfect circle, whereas values approaching 0 indicate increasingly elongated polygons.

To investigate the influence of TMD spatial arrangements on cellular adhesion, the values and distributions of various TMD geometric features at the corresponding sites of downstream cell adhesion (i.e., cell footprint) were first characterized for a sample size of 62 adhered fibroblast cells on WS_2/SiO_2. A diagram demonstrating the procedure for segmenting cellular morphology and corresponding local TMD geometric features can be viewed in Figure 1a−d. Following the characterization of cellular morphology via optical microscope as shown in Figure 1a, cells were removed with trypsin. SEM (Quanta FEG 450, FEI) images were taken to quantify the underlying TMD geometric features, as easily distinguished visually from the underlying SiO_2 substrate by a darker contrast (i.e., conductivity difference). Figure 1b demonstrates a combined image with the optical image (65% transparency) overlaid on the SEM image in Figure 1c, where TMD edges are matched to ensure accuracy of locating a cell footprint and confirm no removal of TMD surfaces post cell removal. To map the geometric properties of the underlying TMD to the resultant cell adhesion behavior, perimeter boxes as in Figure 1d were drawn around a representative adherent fibroblast cell in the optical image shown in Figure 1a and the corresponding cell footprint in the SEM image of the TMD/substrate shown in Figure 1c.

TMD geometric features calculated and defined within Fiji included the following: average Feret diameter, average nearest neighbor distance (NND), average TMD island area, total TMD perimeter, TMD island count, and TMD percent coverage. Individual TMD islands were defined as distinctly isolated TMD, as characterized by SEM. The Feret diameter (i.e., caliper diameter) is defined as the maximum distance between two parallel tangents of the two-dimensional outline of an individual TMD island, selected as a measure

DOI: 10.1021/acsabm.8b00405
ACS Appl. Bio Mater. XXXX, XXX, XXX−XXX

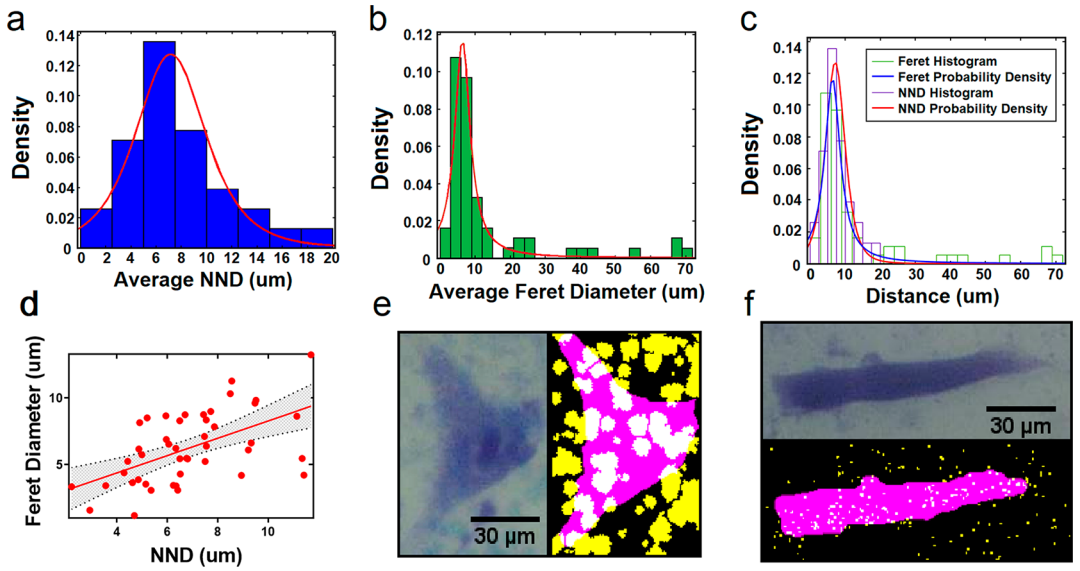

Figure 3. Average nearest neighbor distance and Feret diameter of WS_2 at the fibroblast's cell footprint. Histograms of (a) average NND ($\mu = 7.1496 \pm 0.50653$ μm, $\sigma = 2.92163 \pm 0.636626$ μm) and (b) average Feret diameter ($\mu = 6.3804 \pm 0.524561$ μm and $\sigma = 2.69729 \pm 0.540459$ μm) at the cell footprint graphed with the corresponding *t* location scale distributions and (c) combined. The 95% confidence intervals for average NND and average Feret diameter encompass the range of 1.30634 to 12.99286 μm, and 0.98582 to 11.77498 μm, respectively. A correlation graph of (d) average NND vs average Feret diameter within the 95% confidence intervals of the *t* distribution. Linear regression is shown with a 95% confidence interval shaded in gray. Average NND and average Feret diameter are highly significantly correlated (****$P \leq 0.0001$) with a coefficient of determination of 0.3006 and a slope of linear regression of 0.6493 ± 0.151. Representative cell footprints of (e) relatively large average NND and average Feret diameter, as well as (f) relatively low average NND and average Feret diameter. The cell shown in part e that adhered at a location with larger, more well-distributed WS_2 islands had an average Feret diameter of 13.251 μm and average NND of 11.701 ± 5.0341 μm, whereas the cell footprint corresponding to lower values shown in part f had an average Feret diameter of 0.949 μm and average NND of 3.7515 ± 2.5588 μm.

to evaluate average TMD island size due to TMD island shape irregularity. The average Feret diameter was calculated as the mean of Feret diameters of each TMD island. The average NND represents the distance between each feature centroid and its nearest neighbor's centroid location, in order to determine the effect of the average spacing between TMD islands. We obtained the variable of cell area per TMD island by dividing the total cell area by the TMD island count.

Statistical Analysis. Statistical values presented herein were obtained using well-established algorithms with software, GraphPad Prism 7. The TMD and cell data were graphed, and linear regressions were performed with a 95% confidence interval to determine correlation between individual TMD geometric parameters and resulting cellular morphology. We performed unpaired *t* tests on the mean values of cell area and circularity, and *F*-tests on the variances. The slope of the linear regression line represents the rate of change in the morphometric features as the corresponding geometric feature changes. Thus, higher slopes indicate a greater increase in the morphometric parameter as the geometric parameter increases. Coefficient of determination ("R^2") ranges from zero to one and can be thought of as the fraction of the variance shared between the two variables of interest. Thus, a larger coefficient of determination reflects a better fit of the linear regression line and a stronger correlation between the two variables of interest. Statistical significance is then determined by the *P* value (calculated probability) to determine the degree of significance, such that *$P \leq 0.05$; **$P \leq 0.01$, ***$P \leq 0.001$, ****$P \leq 0.0001$. If the *P* value is sufficiently small, the idea that the correlation is due to random sampling can be rejected.

For histograms shown in Figure 3, a *t* distribution was employed assuming the population distribution of the average NND and Feret diameter is normally distributed, where μ is the mean and σ represents standard deviation. A *t* location scale distribution accurately models data sets which have a significant number of outliers and are heavily populated around the mean. The *t* distribution is symmetric and bell-shaped, like the normal distribution, but has heavier tails, meaning it is more prone to producing values that fall far from its mean. With 62 unique data points, the degrees of freedom were calculated as 61, resulting in a *t* value of 2.000 for average nearest neighbor distance (NND), meaning the 95% confidence interval falls within 2 standard deviations of the mean (μ). The 95% confidence intervals for average NND and average Feret diameter encompasses the range of 1.30634 to 12.99286 μm, and 0.98582 to 11.77498 μm, respectively. Thus, this excludes cell footprints, which are limited to a single TMD island corresponding to an average NND of zero, as well as those which would be labeled as outliers, corresponding to a potentially less predictable and more variable outcome.

RESULTS AND DISCUSSION

Cell Morphology on Differing TMD/Substrate Combinations. Cell culture was performed on both as-grown TMDs (i.e., MoS_2 or WS_2) on SiO_2 and TMDs transferred onto cytocompatible PDMS.[43−45] TMD-free control substrates (i.e., PDMS and SiO_2) were used to test the presence of TMDs on fibroblast cell adhesion, as shown in Figure 2, quantitatively confirming the observation that the presence of TMDs improved cellular adhesion. Fibroblast cells adhering on the control substrates exhibited a significantly smaller cell area and more circular morphology than those in the presence of MoS_2 (****$P \leq 0.0001$ and **$P \leq 0.01$, respectively) and WS_2 (****$P \leq 0.0001$ and **$P \leq 0.01$, respectively), indicating an enhanced cellular adhesion in the presence of TMDs on both SiO_2 and PDMS substrates. (A combined bar graph is shown in Figure S7 for comparison.)

The statistical differences for cell area and circularity calculated between each TMD type and the control sample resulted in *P* values within similar ranges ($P \leq 0.0001$ and $P \leq 0.01$), respectively), suggesting an overall similar effect on the average cellular morphology for WS_2 and MoS_2. There was a more significant difference observed in the cell area ($P \leq 0.0001$) than circularity ($P \leq 0.01$), which demonstrates that the

DOI: 10.1021/acsabm.8b00405
ACS Appl. Bio Mater. XXXX, XXX, XXX−XXX

presence of TMDs greatly increased the total area of adhered cells and resulted in a significantly more elongated cell morphology. The cell morphology was determined to be slightly more elongated on MoS_2 than WS_2 ($P \leq 0.05$) with respect to circularity. Compared to MoS_2, a significantly larger distribution of cell areas was determined for the WS_2 sample. These minor differences observed between MoS_2 and WS_2 are attributed to differences between samples concerning the variable local TMD geometric properties, such as the size and distribution of TMD islands, rather than the type of TMD. Owing to their shared molecular structure and basal planes of both MoS_2 and WS_2 consisting of exterior sulfur, no significant differences exist between MoS_2 and WS_2 in terms of material properties such as their stiffness,[38] hydrophobicity,[46,47] and cytocompatibility.[32−34] Overall, analysis of cellular morphology on both TMD/PDMS and TMD/SiO_2 yielded similar trends with adhered fibroblast cells exhibiting a greater circularity and cell area in the presence of TMDs. Thus, the enhanced cellular adhesion observed with TMDs may indicate not only an efficacy in reversing substrate toxicity but also an ability to confer favorable substrate properties for cell adhesion.

Characterization of TMD Geometric Features at Locations of Cellular Adhesion. All TMD geometric features presented herein are calculated from the segmented areas located under the footprint of the cell. For example, the average NND and average Feret diameter at each cell footprint were calculated, and their distributions are graphed as histograms as shown in Figure 3a,b, respectively, which summarizes the distribution of TMD geometric parameters and the relationship between TMD coverage and the locations of cell adhesion. The data is normally distributed, as evidenced by the overlay of the normal distribution fitted to the histogram.

As shown in Figure 3c, the means and standard deviations of the distributions for an average NND and average Feret diameter are notably similar, with a percent difference of only 11.3703% and 7.98516%, respectively. This similarity suggests that fibroblast cells do not adhere exclusively in areas that are monolithic in their TMD coverage, but rather cells are adhering on surfaces with unconnected TMD islands with exposed underlying cytotoxic SiO_2 at the cell footprint. The correlation between the average NND and average Feret diameter was graphed in Figure 3d, which shows the relationship between TMD geometric properties at the cell footprint and the correlation between the size and spacing of TMD islands, regarding the locations of fibroblast cellular adhesion. The average NND and average Feret diameter are highly significantly correlated ($^{****}P \leq 0.0001$), implying that cells are adhering at heterogeneous locations with TMD islands that are proportionally sized by their spacing. Characterization of local geometric arrangements of TMDs at the cell footprint indicates that fibroblast cells adhere in locations where the spacing between TMD islands decreases as the TMD island size decreases.

This is further illustrated in Figure 3e with a cell footprint pertaining to relatively high average NND and relatively high average Feret diameter, in contrast to Figure 3f with a cell footprint corresponding to TMDs with a relatively low average NND and average Feret diameter. The fibroblast cell shown in Figure 3e that adhered at a location with larger, more well-distributed TMD islands had an average Feret diameter of 13.251 μm and average NND of 11.701 ± 5.0341 μm.

It has been shown that cells migrate over time to regions with more favorable surface properties.[48−50] Due to the observed affinity of fibroblast cells to surfaces with TMDs, cells were expected to preferably adhere similarly to local areas of increasing percent coverage of TMD. However, the fibroblast cells preferred areas that were heterogeneous in areal magnitude, pertaining to TMD islands with exposed underlying substrate, as qualitatively shown in Figure S9. Overall, we observed fewer adhesions in areas that were exclusively SiO_2 or exclusively TMD. To further elucidate the causal relationship of enhanced adhesion in the presence of TMDs, we performed analysis correlating the geometric TMD properties with the cellular morphometric features shown in the following section.

Effects of TMD Geometric Features on Cellular Morphology. A data table summarizing the statistical findings is given in Table 1. In the Supporting Information, Table S1 includes the slope of the linear regression line, which represents the rate of change in the morphometric features as the corresponding geometric feature changes.

Table 1. Summary Table of Statistical Analysis of Correlations: TMD Geometric Features vs Cellular Morphometric Features[a]

		cellular morphometry feature	
TMD geometric parameter	cell area per TMD island	total cell area	circularity
perimeter	0.82 (****)[c]	0.00 (ns)	0.06 (ns)
Feret diameter[b]	0.81 (****)[c]	0.01 (ns)	0.05 (ns)
island area[b]	0.78 (****)[c]	0.00 (ns)	0.05 (ns)
percent coverage	0.38 (****)[c]	0.03 (ns)	0.04 (ns)
total area	0.21 (***)[c]	0.09 (*)[c]	0.31 (****)[c]
island count	0.08 (*)[c]	0.40 (****)[c]	0.10 (*)[c]
NND[b]	0.04 (ns)	0.00 (ns)	0.01 (ns)

[a]Values shown are the calculated coefficients of determination corresponding to each TMD geometric parameter vs each cellular morphometric feature, with the statistical significance shown in parentheses ($^{*}P \leq 0.05$; $^{**}P \leq 0.01$, $^{***}P \leq 0.001$, $^{****}P \leq 0.0001$). [b]Average values corresponding to TMD islands at the cell footprint. [c]Significant correlations between TMD geometric parameters and cellular morphometric features are shown, and TMD geometric parameters are ordered descending from the highest significance to the least with correlations to cell area per TMD island.

As shown in Figure 4, TMD coverage (i.e., total area and percent coverage) was analyzed in relation to the resulting cellular area and circularity. A significant correlation is observed between total TMD area and the morphometric features; a smaller P value ($^{****}P \leq 0.0001$) is observed between the circularity and total TMD area than the cell area ($^{*}P \leq 0.05$), indicating that the increased amount of TMD surface may result in greater cellular elongations. In contrast, performing the same analysis based on variable percent coverage of TMD yielded no significance. Thus, a greater percent coverage of TMD did not correlate to an enhanced cellular adhesion. As a testing parameter, the TMD percent coverage would be more indicative than total TMD coverage; the total TMD area is generally expected to increase with larger, more elongated fibroblast cells that have a larger perimeter box (or area of analysis). Therefore, there is no direct correlation observed between the amount of TMD coverage at the site of cellular adhesion. Instead, additional geometric parameters relating to the spatial arrangement of TMD (rather than the amount of TMD) may play a greater role in the adhesive nature of cells.

To investigate the influence of TMD islands and their dimensions, the remaining geometric features and their correlations to the cellular morphometric features were

DOI: 10.1021/acsabm.8b00405
ACS Appl. Bio Mater. XXXX, XXX, XXX−XXX

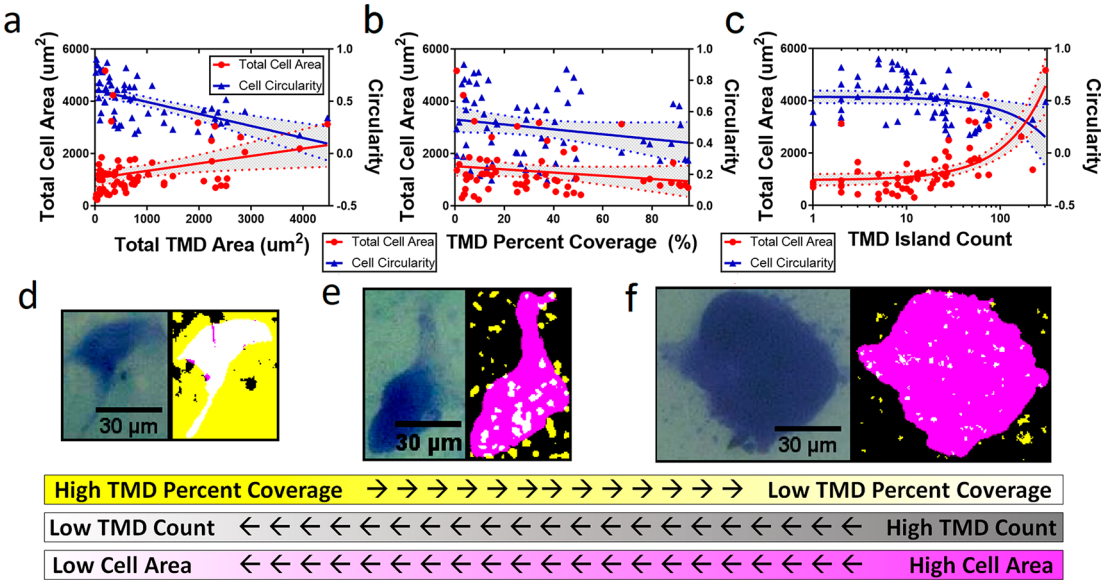

Figure 4. Effects of TMD area parameters on total cell area and circularity of adhered fibroblast cells. Graph of morphometric features of fibroblast cells adhered on WS_2 on SiO_2 compared to TMD geometric parameters: (a) TMD total area vs cell total area (left *y*-axis) and TMD total area vs circularity (right *y*-axis), (b) TMD coverage area vs cell total area (left *y*-axis) and TMD coverage area vs cell circularity (right *y*-axis), and (c) TMD island count vs cell total area (left *y*-axis) and TMD island count vs cell circularity (right *y*-axis) The gray shaded region symmetric about the regression indicates a 95% confidence interval. Representative cell footprints are shown, including (d) low total cell area, high TMD percent coverage, and low TMD count, (e) high total cell area, high TMD percent coverage, and high TMD count, and (f) low TMD percent coverage and high TMD count.

determined, including areal thresholding to determine TMD island count as shown in Figure 4c. For the number of TMD islands, a smaller P value ($^{****}P \leq 0.0001$) was observed between total cell area than the circularity ($^{*}P \leq 0.05$), indicating that the increased number of TMD islands resulted in significantly greater cell areas and slightly more elongations deviating from a circular morphology. The coefficient of determination was relatively high (0.4043) between the number of TMD islands and the cell total area, whereas the coefficient of determination was lower (0.0951) between the number of TMD islands and the cell circularity.

To further illustrate this finding, Figure 4d represents a cell footprint with a high percent coverage of TMD that results in a relatively low total cell area. As the TMD count increases, an overall greater cell area and lower circularity (i.e., greater cytoplasmic elongations) are generally observed. This finding is independent of total TMD coverage as shown in Figure 4e by a cell footprint that contains a lower TMD percent coverage and higher TMD count than in Figure 4d. The cell footprint in Figure 4f correlates to an even bigger cell area, with an even lower TMD percent coverage. The corresponding values are compiled in Table 2.

Significant correlations were observed between morphometric features and TMD geometric features for two out of the six studied geometric parameters (i.e., total TMD area and TMD island count). TMD island count resulted in the correlation of highest significance with cellular area (i.e., extent of cellular spread). Each TMD geometric property was compared with the cellular area per TMD island, in effect normalizing the influence of the strongly correlated TMD count to obtain a more accurate portrayal of the correlations of cellular morphology with geometric features apart from TMD island count. Following the normalization of cell area by the TMD count, high correlations were found with the TMD geometric properties as shown in Figure 5a–f. Therefore, the cell area per TMD was significantly correlated to the average Feret diameter, when

Table 2. Summary Table of TMD Geometric Features and Cellular Morphometric Features Corresponding to Images in Figure 4[a]

	metrology				
	cellular morphometric feature		TMD geometric parameter		
cell-TMD image	total cell area (μm^2)	circularity	TMD count	TMD percent coverage	total TMD area (μm^2)
Figure 4d	816.26	0.637	6	91.003	753.564
Figure 4e	1735.517	0.246	59	12.987	428.063
Figure 4f	3238	0.656	46	7.801	311.725

[a]The values of the cell footprint corresponding to Figure 4d include a total cell area of 816.26 μm^2, circularity of 0.637, TMD percent coverage of 91.003%, TMD count of 6, and total TMD area of 753.564 μm^2. Figure 4e represents a cell footprint that contains a lower TMD percent coverage and higher TMD count than the cell footprint in Figure 4d and results in an overall greater cell area and lower circularity (i.e., greater cytoplasmic elongations). The corresponding values of Figure 4e include total cell area of 1735.517 μm^2, circularity of 0.246, TMD percent coverage of 12.987%, TMD count of 59, and a total TMD area of 428.063 μm^2. The cell footprint in Figure 4f correlates to an even bigger cell area, with an even lower TMD percent coverage. The corresponding values are the total cell area of 3238 μm^2, circularity of 0.656, TMD percent coverage of 7.801%, TMD count of 46, and total TMD area of 311.725 μm^2.

taking into consideration the TMD island count. The same phenomenon was observed with an average TMD island area, total TMD perimeter, and TMD percent coverage. As observed, each TMD island parameter except for average NND was significantly correlated to the resulting cellular area per TMD count. Therefore, the resulting morphology of cells on diverse substrates could potentially be manipulated by tailoring the geometric parameters of TMDs, even on substrates that are

DOI: 10.1021/acsabm.8b00405
ACS Appl. Bio Mater. XXXX, XXX, XXX−XXX

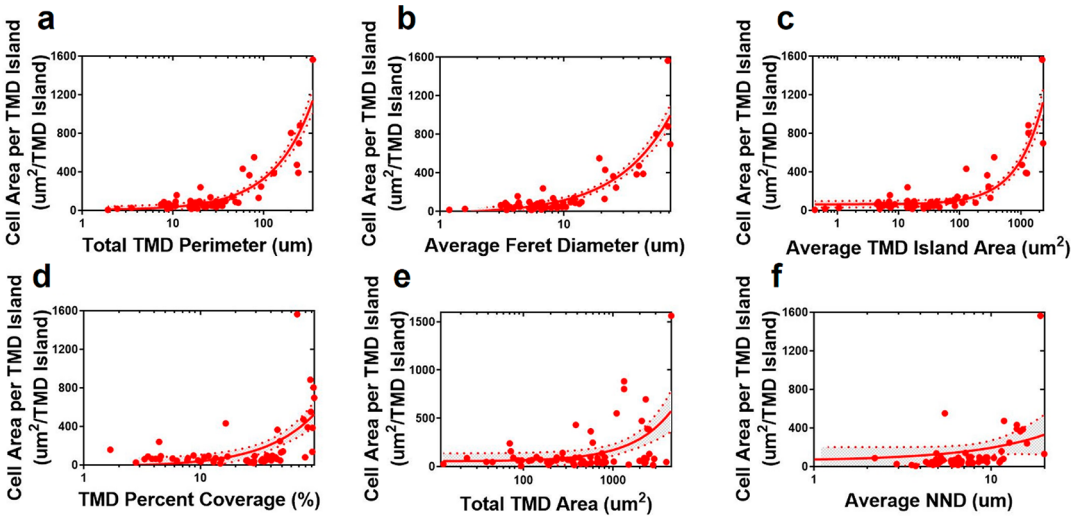

Figure 5. Effects of TMD geometric properties to normalization of cell area with respect to TMD island count. Graph of cellular area per TMD of fibroblast cells adhered on WS_2/SiO_2 compared to TMD geometric parameters, descending from most highly correlated to least correlated: (a) total TMD perimeter vs cell area per TMD island, (b) average Feret diameter vs cell area per TMD island, (c) average TMD island vs cell area per TMD island, (d) TMD percent coverage vs cell area per TMD island, (e) total TMD area vs cell area per TMD island, (f) average NND vs cell area per TMD island. The gray shaded region symmetric about the line of regression indicates a 95% confidence interval. Despite the number of TMD islands underlying the cell footprint, the average Feret diameter, average TMD island area, total TMD area, total TMD perimeter, and TMD percent coverage were significantly correlated to the cell area per TMD; the statistical significance relating to these correlations can be viewed in Table 1.

cytotoxic and adverse to cellular adhesion. Cellular adhesion ultimately influences cellular survival, proliferation, differentiation, and migration, and the TMDs' affinity to cellular adhesion coupled with its unique electronic and chemical properties can be further explored and applied in biomedical fields that utilize 2D cell cultures.

Monolayer TMD surfaces confer a lower roughness,[51] higher hydrophobicity,[46,47] and higher stiffness[38,52] in comparison to underlying SiO_2. It has been known that monolayer TMDs on substrates have a stiffness proportional to their underlying substrate stiffness.[52−54] For example, CVD monolayer MoS_2 and WS_2 have similarly high 2D elastic moduli, ∼270 GPa, whereas the elastic modulus of SiO_2 is ∼70 GPa.[38] PDMS resulted in a lower average cell area than SiO_2 counterparts, since PDMS is less stiff (∼2.6 GPa)[55] and more hydrophobic than both SiO_2 and TMD,[56,57] and cells develop a greater attachment and spreading on hydrophilic[58] and stiffer substrates.[50,59] As observed, the presence of TMDs enhanced cell morphology on both SiO_2 and PDMS. Cells cultured on TMD surfaces attach and move across monolayers,[60] and the cellular movement cycle includes the following stages: unbound, rolling, tumbling, transient adhesion, and adhesion.[61] Since TMDs conform to substrate topography and are proportionally less rough (i.e., less friction) than SiO_2,[51] cells seeded directly on TMDs undergo a greater degree of rolling/tumbling and higher observed cell adhesion in heterogeneous regions (i.e., with contributions of SiO_2, not monolithic TMDs), where cells slowed to transient adhesion due to a higher friction and hydrophilic tendency.[58] Furthermore, we observe an enhanced morphology in heterogeneous regions with an increasing TMD island count following transient adhesion due to increased local TMD islands of a high stiffness and elongations past SiO_2. We attribute this to cell movement toward more rigid surfaces,[59] within critical distances comparable to the cell size.[62,63] Cells bind to surface adsorbed proteins from culture media,[64−66] and TMDs exhibit a high physical adsorption of organic macromolecules due to a large surface area, no dangling bonds, and van der Waals affinity.[20,67] In the absence of strong ionic or covalent bonding sites, proteins collect on TMDs, forming concentrated reservoirs of surface proteins. In combination with TMD high stiffness, cells then spread to TMD surfaces of greater surface parameters within a sensible range, as observed by the positive correlations between cell area per TMD island and TMD island size parameters.

The findings presented herein give insight on the effects of distribution of TMDs on cell adhesion and morphology. This understanding will allow for tailoring the adhesion of cells on diverse substrates (even those inherently adverse or cytotoxic to cells), which can be guided by geometric parameters of TMDs. Therefore, it could ultimately be used to influence and control cellular survival, proliferation, differentiation, and migration. By taking advantage of unique optical and electronic properties of TMDs, one could further utilize this understanding toward tissue scaffolds, stem cell differentiation, and live-cell biosensing applications

CONCLUSIONS

We have demonstrated that TMD presence improved cellular adhesion on substrates, including cytocompatible PDMS and cytotoxic SiO_2, and quantitatively analyzed the cell morphometric features, determining the statistical significance. We found that TMD surfaces in an arbitrary order can be used to enhance cell adhesion on substrates that are inert to cell attachment, rendering otherwise cytotoxic substrates useful as 2D cell culture platforms. TMD intersample variability indicated that additional local surface parameters affect cell adhesion. The measured similarity between the average Feret diameter and NND distributions suggests that cells do not only adhere to monolithic TMD coverage areas but also on surfaces composed of unconnected TMD islands with exposed underlying SiO_2 at the cell footprint. We surmised cells seeded directly on TMDs undergo a greater degree of rolling/tumbling and higher observed cell adhesion in heterogeneous regions (i.e., with contributions of SiO_2, not monolithic TMDs), where cells

DOI: 10.1021/acsabm.8b00405
ACS Appl. Bio Mater. XXXX, XXX, XXX−XXX

slowed to transient adhesion due to a higher friction and hydrophilic tendency. We found that quantitative increases in the TMD island count correlated to significantly larger, elongated cells. Further, the cell area per TMD island resulted in significant positive correlations with total TMD perimeter, average Feret diameter, average TMD island area, and TMD percent coverage. This implies that the number of underlying TMDs is the strongest correlation with TMD geometric arrangements that are distributed within the range of TMD sample geometric parameters characterized. We attribute observably enhanced morphology in heterogeneous regions with an increasing TMD island count and size due to increased local TMD islands of a high stiffness and elongations past SiO_2, within critical distances comparable to the cell size; in combination, TMD favorable adsorption of proteins from cell media results in time-dependent adsorbent concentrations at TMD islands, critical to the promotion of cell adhesion and enhanced morphology. By tailoring the geometric parameters of TMDs, one can guide the desirable adhesion of cells on diverse substrates (even those inherently adverse or cytotoxic to cells), which ultimately influences cellular survival, proliferation, differentiation, and migration; these findings can be further explored and applied in fields that utilize cell cultures toward biomedical applications, including tissue scaffolds, stem cell differentiation, and live-cell biosensing applications.

■ ASSOCIATED CONTENT

Supporting Information

The Supporting Information is available free of charge on the ACS Publications website at DOI: 10.1021/acsabm.8b00405.

Details of the Raman and photoluminescence characterization of TMD, flowchart of the TMD sample fabrication and transfer method, before and after cell culturing imaging on TMD, cell stain concentration, cell stain time of exposure, cell segmentation for analysis of morphometric features, bar graphs of morphometric features of fibroblast cells on differing substrates, linear regression and correlation of TMD geometric features relating to cell morphology and cell area per TMD island, residual plots of linear regressions of each combination of TMD geometric property and morphometric feature, and summary table of statistical analysis of correlation and linear regression of TMD geometric features vs cellular morphometric features (PDF)

■ AUTHOR INFORMATION

Corresponding Author

*E-mail: eyang@stevens.edu.

ORCID

Eui-Hyeok Yang: 0000-0003-4893-1691

Funding

This work was supported in part by the National Science Foundation award (CMMI-1554150) and Air Force Office of Scientific Research award (FA9550-12-1-0326). This work was also partially carried out at the Micro Device Laboratory. Anthony Palumbo was supported by the I&E Doctoral Fellowship at the Stevens Institute of Technology.

Notes

The authors declare no competing financial interest.

■ ACKNOWLEDGMENTS

The authors thank Houzhu Ding for his assistance in maintaining the laboratory for cell culture procedures. The authors would also like to thank Kyungnam Kang, Shichen Fu, and Xiaotian Wang for helpful discussion on the growth of TMDs.

■ ABBREVIATIONS

2D, two-dimensional; CVD, chemical vapor deposition; KOH, potassium oxide; MoS_2, molybdenum disulfide; NHDF, neonatal human dermal fibroblast; NND, nearest neighbor distance; OM, optical microscope; PDMS, polydimethylsiloxane; PMMA, poly(methyl methacrylate); SEM, scanning electron microscopy; SiO_2, silicon dioxide; WS_2, tungsten disulfide

■ REFERENCES

(1) Lv, R.; Robinson, J. A.; Schaak, R. E.; Sun, D.; Sun, Y.; Mallouk, T. E.; Terrones, M. Transition Metal Dichalcogenides and beyond: Synthesis, Properties, and Applications of Single- and Few-Layer Nanosheets. *Acc. Chem. Res.* **2015**, *48* (1), 56−64.

(2) Kuc, A.; Heine, T.; Kis, A. Electronic Properties of Transition-Metal Dichalcogenides. *MRS Bull.* **2015**, *40* (7), 577−584.

(3) Chhowalla, M.; Shin, H. S.; Eda, G.; Li, L.-J.; Loh, K. P.; Zhang, H. The Chemistry of Two-Dimensional Layered Transition Metal Dichalcogenide Nanosheets. *Nat. Chem.* **2013**, *5* (4), 263−275.

(4) Wang, Q. H.; Kalantar-Zadeh, K.; Kis, A.; Coleman, J. N.; Strano, M. S. Electronics and Optoelectronics of Two-Dimensional Transition Metal Dichalcogenides. *Nat. Nanotechnol.* **2012**, *7* (11), 699−712.

(5) Kang, K. N.; Godin, K.; Kim, Y. D.; Fu, S.; Cha, W.; Hone, J.; Yang, E. H. Graphene-Assisted Antioxidation of Tungsten Disulfide Monolayers: Substrate and Electric-Field Effect. *Adv. Mater.* **2017**, *29* (18), 1603898.

(6) Kang, K. N.; Godin, K.; Yang, E. H. The Growth Scale and Kinetics of WS_2 Monolayers under Varying H_2 Concentration. *Sci. Rep.* **2015**, *5*, 13205.

(7) Schneider, L. M.; Lippert, S.; Kuhnert, J.; Renaud, D.; Kang, K. N.; Ajayi, O.; Halbich, M.-U.; Abdulmunem, O. M.; Lin, X.; Hassoon, K.; Edalati-Boostan, S.; Kim, T. D.; Heimbrodt, W.; Yang, E. H.; Hone, J. C.; Rahimi-Iman, A. The Impact of the Substrate Material on the Optical Properties of 2D WSe_2 Monolayers. *Semiconductors* **2018**, *52* (5), 565−571.

(8) Huang, Y.; Shi, Y.; Yang, H. Y.; Ai, Y. A Novel Single-Layered MoS_2 Nanosheet Based Microfluidic Biosensor for Ultrasensitive Detection of DNA. *Nanoscale* **2015**, *7* (6), 2245−2249.

(9) Lee, D. W.; Lee, J.; Sohn, I. Y.; Kim, B. Y.; Son, Y. M.; Bark, H.; Jung, J.; Choi, M.; Kim, T. H.; Lee, C.; Lee, N. E. Field-Effect Transistor with a Chemically Synthesized MoS_2 Sensing Channel for Label-Free and Highly Sensitive Electrical Detection of DNA Hybridization. *Nano Res.* **2015**, *8* (7), 2340−2350.

(10) Splendiani, A.; Sun, L.; Zhang, Y.; Li, T.; Kim, J.; Chim, C. Y.; Galli, G.; Wang, F. Emerging Photoluminescence in Monolayer MoS_2. *Nano Lett.* **2010**, *10* (4), 1271−1275.

(11) Sarkar, D.; Liu, W.; Xie, X.; Anselmo, A. C.; Mitragotri, S.; Banerjee, K. MoS_2 Field-Effect Transistor for next-Generation Label-Free Biosensors. *ACS Nano* **2014**, *8* (4), 3992−4003.

(12) Farimani, A. B.; Min, K.; Aluru, N. R. DNA Base Detection Using a Single-Layer MoS_2. *ACS Nano* **2014**, *8* (8), 7914−7922.

(13) Schneider, G. F.; Kowalczyk, S. W.; Calado, V. E.; Pandraud, G.; Zandbergen, H. W.; Vandersypen, L. M. K.; Dekker, C. DNA Translocation through Graphene Nanopores. *Nano Lett.* **2010**, *10* (8), 3163−3167.

(14) Yong, Y.; Zhou, L.; Gu, Z.; Yan, L.; Tian, G.; Zheng, X.; Liu, X.; Zhang, X.; Shi, J.; Cong, W.; Yin, W.; Zhao, Y. WS_2 Nanosheet as a New Photosensitizer Carrier for Combined Photodynamic and Photothermal Therapy of Cancer Cells. *Nanoscale* **2014**, *6* (17), 10394−10403.

DOI: 10.1021/acsabm.8b00405
ACS Appl. Bio Mater. XXXX, XXX, XXX−XXX

(15) Cheng, L.; Liu, J.; Gu, X.; Gong, H.; Shi, X.; Liu, T.; Wang, C.; Wang, X.; Liu, G.; Xing, H.; Bu, W.; Sun, B.; Liu, Z. PEGylated WS_2 Nanosheets as a Multifunctional Theranostic Agent for in Vivo Dual-Modal CT/Photoacoustic Imaging Guided Photothermal Therapy. *Adv. Mater.* **2014**, *26* (12), 1886−1893.
(16) Kalantar-zadeh, K.; Ou, J. Z.; Daeneke, T.; Strano, M. S.; Pumera, M.; Gras, S. L. Two-Dimensional Transition Metal Dichalcogenides in Biosystems. *Adv. Funct. Mater.* **2015**, *25* (32), 5086−5099.
(17) Chen, Y.; Tan, C.; Zhang, H.; Wang, L. Two-Dimensional Graphene Analogues for Biomedical Applications. *Chem. Soc. Rev.* **2015**, *44* (9), 2681−2701.
(18) Chimene, D.; Alge, D. L.; Gaharwar, A. K. Two-Dimensional Nanomaterials for Biomedical Applications: Emerging Trends and Future Prospects. *Adv. Mater.* **2015**, *27* (45), 7261−7284.
(19) Li, Z.; Wong, S. L. Functionalization of 2D Transition Metal Dichalcogenides for Biomedical Applications. *Mater. Sci. Eng., C* **2017**, *70*, 1095−1106.
(20) Kalantar-zadeh, K.; Ou, J. Z. Biosensors Based on Two-Dimensional MoS_2. *ACS Sensors* **2016**, *1* (1), 5−16.
(21) Pumera, M.; Loo, A. H. Layered Transition-Metal Dichalcogenides (MoS_2 and WS_2) for Sensing and Biosensing. *TrAC, Trends Anal. Chem.* **2014**, *61*, 49−53.
(22) Wang; Shu, J.; Qiu, W.; Guo, X.; Yu, J.; Nie, J.; Zhang, X.; Zhang, Z.; Liu, X.; Mou, L.; Li, H. L. A Nanostructured Molybdenum Disulfide Film for Promoting Neural Stem Cell Neuronal Differentiation: Toward a Nerve Tissue-Engineered 3D Scaffold. *Adv. Biosyst.* **2017**, *1* (5), 1600042.
(23) Lalwani, G.; Henslee, A. M.; Farshid, B.; Lin, L.; Kasper, F. K.; Qin, Y.; Mikos, A. G.; Sitharaman, B. Two-Dimensional Nanostructure-Reinforced Biodegradable Polymeric Nanocomposites for Bone Tissue Engineering. *Biomacromolecules* **2013**, *14* (3), 900−909.
(24) Shuai, C.; Sun, H.; Gao, C.; Feng, P.; Guo, W.; Yang, Y.; Zhao, M.; Yang, S.; Yuan, F.; Peng, S. Mechanical Reinforcement of Bioceramics Scaffolds via Fracture Energy Dissipation Induced by Sliding Action of MoS_2 Nanoplatelets. *J. Mech. Behav. Biomed. Mater.* **2017**, *75*, 423−433.
(25) Wang, X.; Li, T.; Ma, H.; Zhai, D.; Jiang, C.; Chang, J.; Wang, J.; Wu, C. A 3D-Printed Scaffold with MoS2 Nanosheets for Tumor Therapy and Tissue Regeneration. *NPG Asia Mater.* **2017**, *9* (4), e376.
(26) Gumbiner, B. M. Cell Adhesion: The Molecular Basis of Tissue Architecture and Morphogenesis. *Cell* **1996**, *84* (3), 345−357.
(27) Bhimanapati, G. R.; Lin, Z.; Meunier, V.; Jung, Y.; Cha, J.; Das, S.; Xiao, D.; Son, Y.; Strano, X. M. S.; Cooper, X. V. R.; Liang, O. L.; Louie, S. G.; Ringe, E.; Zhou, W.; Kim, O. S. S.; Naik, R. R.; Sumpter, B. G.; Terrones, O. H.; Xia, F.; Wang, Y.; Zhu, J.; Akinwande, D.; Alem, N.; Schuller, J. A.; Schaak, R. E.; Terrones, Â. M.; Robinson, J. A. Recent Advances in Two-Dimensional Materials beyond Graphene. *ACS Nano* **2015**, *9* (12), 11509−11539.
(28) Bajaj, P.; Rivera, J. A.; Marchwiany, D.; Solovyeva, V.; Bashir, R. Graphene-Based Patterning and Differentiation of C2C12 Myoblasts. *Adv. Healthcare Mater.* **2014**, *3* (7), 995−1000.
(29) Redlich, M.; Katz, A.; Rapoport, L.; Wagner, H. D.; Feldman, Y.; Tenne, R. Improved Orthodontic Stainless Steel Wires Coated with Inorganic Fullerene-like Nanoparticles of WS_2 Impregnated in Electroless Nickel-Phosphorous Film. *Dent. Mater.* **2008**, *24* (12), 1640−1646.
(30) Wu, H.; Yang, R.; Song, B.; Han, Q.; Li, J.; Zhang, Y.; Fang, Y.; Tenne, R.; Wang, C. Biocompatible Inorganic Fullerene-like Molybdenum Disulfide Nanoparticles Produced by Pulsed Laser Ablation in Water. *ACS Nano* **2011**, *5* (2), 1276−1281.
(31) Goldman, E. B.; Zak, A.; Tenne, R.; Kartvelishvily, E.; Levin-Zaidman, S.; Neumann, Y.; Stiubea-Cohen, R.; Palmon, A.; Hovav, A.-H.; Aframian, D. J. Biocompatibility of Tungsten Disulfide Inorganic Nanotubes and Fullerene-like Nanoparticles with Salivary Gland Cells. *Tissue Eng., Part A* **2015**, *21* (5−6), 1013−1023.
(32) Teo, W. Z.; Chng, E. L. K.; Sofer, Z.; Pumera, M. Cytotoxicity of Exfoliated Transition-Metal Dichalcogenides (MoS_2, WS_2, and WSe_2) Is Lower than That of Graphene and Its Analogues. *Chem. - Eur. J.* **2014**, *20* (31), 9627−9632.
(33) Shah, P.; Narayanan, T. N.; Li, C.-Z.; Alwarappan, S. Probing the Biocompatibility of MoS_2 Nanosheets by Cytotoxicity Assay and Electrical Impedance Spectroscopy. *Nanotechnology* **2015**, *26* (31), 315102.
(34) Appel, J. H.; Li, D. O.; Podlevsky, J. D.; Debnath, A.; Green, A. A.; Wang, Q. H.; Chae, J. Low Cytotoxicity and Genotoxicity of Two-Dimensional MoS_2 and WS_2. *ACS Biomater. Sci. Eng.* **2016**, *2* (3), 361−367.
(35) Suhito, I. R.; Han, Y.; Kim, D.; Son, H.; Kim, T. Effects of Two-Dimensional Materials on Human Mesenchymal Stem Cell Behaviors. *Biochem. Biophys. Res. Commun.* **2017**, *493* (1), 578−584.
(36) Mohammad Tabatabaei, S.; Noei, M.; Khaliji, K.; Pourfath, M.; Fathipour, M. A First-Principles Study on the Effect of Biaxial Strain on the Ultimate Performance of Monolayer MoS_2-Based Double Gate Field Effect Transistor. *J. Appl. Phys.* **2013**, *113* (16), 1−6.
(37) Conley, H. J.; Wang, B.; Ziegler, J. I.; Haglund, R. F.; Pantelides, S. T.; Bolotin, K. I. Bandgap Engineering of Strained Monolayer and Bilayer MoS_2. *Nano Lett.* **2013**, *13* (8), 3626−3630.
(38) Liu, K.; Yan, Q.; Chen, M.; Fan, W.; Sun, Y.; Suh, J.; Fu, D.; Lee, S.; Zhou, J.; Tongay, S.; Ji, J.; Neaton, J. B.; Wu, J. Elastic Properties of Chemical-Vapor-Deposited Monolayer MoS_2, WS_2, and Their Bilayer Heteostructures. *Nano Lett.* **2014**, *14* (9), 5097−5103.
(39) Choi, J. H.; Zhang, H. Y.; Du, H. D.; Choi, J. H. Understanding Solvent Effects on the Properties of Two-Dimensional Transition Metal Dichalcogenides. *ACS Appl. Mater. Interfaces* **2016**, *8* (14), 8864−8869.
(40) Tongay, S.; Zhou, J.; Ataca, C.; Liu, J.; Kang, J. S.; Matthews, T. S.; You, L.; Li, J. B.; Grossman, J. C.; Wu, J. Q. Broad-Range Modulation of Light Emission in Two-Dimensional Semiconductors by Molecular Physisorption Gating. *Nano Lett.* **2013**, *13* (6), 2831−2836.
(41) Iberi, V.; Liang, L.; Ievlev, A. V.; Stanford, M. G.; Lin, M.-W.; Li, X.; Mahjouri-Samani, M.; Jesse, S.; Sumpter, B. G.; Kalinin, S. V.; Joy, D. C.; Xiao, K.; Belianinov, A.; Ovchinnikova, O. S. Nanoforging Single Layer $MoSe_2$ Through Defect Engineering with Focused Helium Ion Beams. *Sci. Rep.* **2016**, *6* (1), 30481.
(42) Schindelin, J.; Arganda-carreras, I.; Frise, E.; Kaynig, V.; Longair, M.; Pietzsch, T.; Preibisch, S.; Rueden, C.; Saalfeld, S.; Schmid, B.; Tinevez, J.; White, D. J.; Hartenstein, V.; Eliceiri, K.; Tomancak, P.; Cardona, A. Fiji : An Open-Source Platform for Biological-Image Analysis. *Nat. Methods* **2012**, *9* (7), 676−682.
(43) Fujii, T. PDMS-Based Microfluidic Devices for Biomedical Applications. *Microelectron. Eng.* **2002**, *61*, 907−914.
(44) Wu, M.; Huang, S.; Lee, G. Microfluidic Cell Culture Systems for Drug Research. *Lab Chip* **2010**, *10* (8), 939−956.
(45) Zhang, H.; Chiao, M. Anti-Fouling Coatings of Poly-(Dimethylsiloxane) Devices for Biological and Biomedical Applications. *J. Med. Biol. Eng.* **2015**, *35*, 143−155.
(46) Chow, P. K.; Singh, E.; Cruz Viana, B.; Gao, J.; Luo, J.; Li, J.; Lin, Z.; Elias, A. L.; Shi, Y.; Wang, Z.; Terrones, M.; Koratkar, N. Wetting of Mono and Few-Layered WS_2 and MoS_2 Films Supported on Si/SiO_2 Substrates. *ACS Nano* **2015**, *9* (3), 3023−3031.
(47) Kozbial, A.; Gong, X.; Liu, H.; Li, L. Understanding the Intrinsic Water Wettability of Molybdenum Disulfide (MoS_2). *Langmuir* **2015**, *31* (30), 8429−8435.
(48) Lu, J.; Rao, M. P.; MacDonald, N. C.; Khang, D.; Webster, T. J. Improved Endothelial Cell Adhesion and Proliferation on Patterned Titanium Surfaces with Rationally Designed, Micrometer to Nanometer Features. *Acta Biomater.* **2008**, *4* (1), 192−201.
(49) Keshavan, S.; Oropesa-Nunez, R.; Diaspro, A.; Canale, C.; Dante, S. Adhesion and Migration of CHO Cells on Micropatterned Single Layer Graphene. *2D Mater.* **2017**, *4* (2), 025022.
(50) Yeung, T.; Georges, P. C.; Flanagan, L. A.; Marg, B.; Ortiz, M.; Funaki, M.; Zahir, N.; Ming, W.; Weaver, V.; Janmey, P. A. Effects of Substrate Stiffness on Cell Morphology, Cytoskeletal Structure, and Adhesion. *Cell Motil. Cytoskeleton* **2005**, *60* (1), 24−34.
(51) Quereda, J.; Castellanos-Gomez, A.; Agraït, N.; Rubio-Bollinger, G. Single-Layer MoS_2 Roughness and Sliding Friction Quenching by Interaction with Atomically Flat Substrates. *Appl. Phys. Lett.* **2014**, *105* (5), 2−7.

DOI: 10.1021/acsabm.8b00405
ACS Appl. Bio Mater. XXXX, XXX, XXX−XXX

(52) Kim, M. T. Influence of Substrates on the Elastic Reaction of Films for the Microindentation Tests. *Thin Solid Films* **1996**, *283* (1−2), 12−16.
(53) Liu, K.; Yan, Q.; Chen, M.; Fan, W.; Sun, Y.; Suh, J.; Fu, D.; Lee, S.; Zhou, J.; Tongay, S.; Ji, J.; Neaton, B.; Wu, J. Elastic Properties of Chemical-Vapor-Deposited Monolayer MoS_2, WS_2, and Their Bilayer Heterostructures. *Nano Lett.* **2014**, *14*, 5097−5103.
(54) Wang, Z.; Volinsky, A. A.; Gallant, N. D. Crosslinking Effect on Polydimethylsiloxane Elastic Modulus Measured by Custom-Built Compression Instrument. *J. Appl. Polym. Sci.* **2014**, *131* (22), 1−4.
(55) Fuard, D.; Tzvetkova-Chevolleau, T.; Decossas, S.; Tracqui, P.; Schiavone, P. Optimization of Poly-Di-Methyl-Siloxane (PDMS) Substrates for Studying Cellular Adhesion and Motility. *Microelectron. Eng.* **2008**, *85* (5−6), 1289−1293.
(56) Mata, A.; Fleischman, A. J. Characterization of Polydimethylsiloxane (PDMS) Properties for Biomedical Micro/Nanosystems. *Biomed. Microdevices* **2005**, *7* (4), 281−293.
(57) Fromherz, P. Three Levels of Neuroelectronic Interfacing: Silicon Chips with Ion Channels, Nerve Cells, and Brain Tissue. *Ann. N. Y. Acad. Sci.* **2006**, *1093* (1), 143−160.
(58) Webb, K.; Hlady, V.; Tresco, P. A. Relative Importance of Surface Wettability and Charged Functional Groups on NIH 3T3 Fibroblast Attachment, Spreading, and Cytoskeletal Organization. *J. Biomed. Mater. Res.* **1998**, *41* (3), 422−430.
(59) Lo, C.; Wang, H.; Dembo, M.; Wang, Y. Cell Movement Is Guided by the Rigidity of the Substrate. *Biophys. J.* **2000**, *79* (1), 144−152.
(60) Yeh, Y.; Tang, Y.; Lin, Z.; Fujisawa, K.; Lei, Y.; Zhou, Y.; Elías, A. L.; Zheng, S.; Mao, Y.; Liu, Z.; Lu, H.; Terrones, M. Light-Emitting Transition Metal Dichalcogenide Monolayers under Cellular Digestion. *Adv. Mater.* **2018**, *30* (8), 1703321.
(61) Hammer, D. A.; Apte, S. M. Simulation of Cell Rolling and Adhesion on Surfaces in Shear Flow: General Results and Analysis of Selectin-Mediated Neutrophil Adhesion. *Biophys. J.* **1992**, *63* (1), 35−57.
(62) He, S.; Su, Y.; Ji, B.; Gao, H. Some Basic Questions on Mechanosensing in Cell − Substrate Interaction. *J. Mech. Phys. Solids* **2014**, *70*, 116−135.
(63) Dufrene, Y. F.; Pelling, A. E. Force Nanoscopy of Cell Mechanics and Cell Adhesion. *Nanoscale* **2013**, *5* (10), 4094−4104.
(64) Kasemo, B.; Lausmaa, J. Material-Tissue Interfaces: The Role of Surface Properties and Processes. *Environ. Health Perspect.* **1994**, *102* (Suppl 5), 41−45.
(65) Bacakova, L.; Filova, E.; Rypacek, F.; Svorcik, V.; Stary, V. Cell Adhesion on Artificial Materials for Tissue Engineering. *Physiol. Res.* **2004**, *53* (Suppl 1), S35−S45.
(66) Oliveira, S. M.; Song, W.; Alves, M. Chemical Modification of Bioinspired Superhydrophobic Polystyrene Surfaces to Control Cell Attachment/Proliferation. *Soft Matter* **2011**, *7* (19), 8932−8941.
(67) Perkins, F. K.; Friedman, A. L.; Cobas, E.; Campbell, P. M.; Jernigan, G. G.; Jonker, B. T. Chemical Vapor Sensing with Monolayer MoS_2. *Nano Lett.* **2013**, *13* (2), 668−673.

DOI: 10.1021/acsabm.8b00405
ACS Appl. Bio Mater. XXXX, XXX, XXX−XXX